# Enhancing Power Quality in Grid-Connected Fuel Cell Systems Using the Gradient-Based Optimizer

Mohammad Golam Mostafa[1,2,*], Nor Zaihar bin Yahaya[1], Ramani Kannan[1], and Nursyarizal bin Mohd Nor[1]
[1] Department of Electrical and Electronics Engineering, Universiti Teknologi PETRONAS, 32610 Perak, Malaysia
[2] Department of Electrical and Electronic Engineering, World University of Bangladesh, Dhaka, Bangladesh
Email: mostafauap@gmail.com (M.G.M.), norzaihar_yahaya@utp.edu.my (N.Z.B.Y.),
ramani.kannan@utp.edu.my (R.K.), nursyarizal_mnor@utp.edu.my (N.B.M.N.)

Manuscript received September 29, 2025; revised November 6, 2025; accepted December 13, 2025
*Corresponding author

***Abstract*—Recent studies on Energy Management Systems (EMS) have focused on enhancing fuel cell-integrated grid systems. Effective power electronics control strategies for such systems should be easy to implement, capable of minimizing harmonic distortion, and robust under weak grid conditions. However, weak grids present significant challenges, including elevated Total Harmonic Distortion (THD), voltage fluctuations, harmonics from nonlinear loads, and frequency deviations. To address these issues, this paper proposes advanced EMS control strategies optimized using the Gradient-Based Optimized-Proportional Integral (GBO-PI) controller for fuel cell-integrated microgrid systems. The performance of the proposed GBO-PI controller is assessed using two analytical frameworks: THD, convergence analyses, and the transient response of the Direct Current (DC) link voltage under both fixed and variable load conditions. This algorithm has optimized advanced control strategies for EMS in fuel cell-integrated grid systems to enhance the DC link voltage, improving transient response and power quality. The proposed method yields a THD of 0.60%. Moreover, the GBO-PI outperformed other recently developed algorithms by a large margin in terms of settling time and overshoot. The findings demonstrate that the proposed control strategy can enhance fuel cell microgrid integration by improving robustness and sustainability, while effectively managing dynamic load variations and ensuring stable power injection into the electrical grid.**

***Index Terms*—Direct Current (DC)-link voltage control, fuel cell, gradient-based optimizer, grid, hydrogen, optimization algorithm, Total Harmonic Distortion (THD)**

## I. Introduction

The rapid evolution of technology on a global scale increasingly highlights the critical demand for energy. In response, significant research efforts are directed toward renewable energy technologies, with particular emphasis on hydrogen fuel cells, which are projected to serve as a key contributor to future sustainable energy systems [1]. It offers clean utilization, high efficiency, and significant potential for enabling the clean energy transition [2]. Hydrogen fuel cells, recognized for their noiseless operation, present a sustainable and efficient solution to meet future energy demands. The Proton Exchange Membrane Fuel Cell (PEMFC) stands out for its low-temperature operation, impressive power density, and efficiency. Additionally, it features quick startup, flexible fuel input, and a compact design. Hydrogen energy addresses the intermittency of renewable sources like wind and solar, enhancing power flow stability, with notable advancements in integrating fuel cells into electrical networks and microgrids [3].

Microgrids have emerged as a crucial component of modern power systems, enabling localized energy management and high integration of Renewable Energy Sources (RESs). Nevertheless, maintaining voltage and frequency stability remains a significant challenge, primarily due to the intermittent characteristics of RESs, dynamic load variations, and disturbances arising from grid interactions [4]. Additionally, microgrids must maintain stable power delivery with minimal harmonic distortion to fully optimize the use of renewable energy sources. However, integrating nonlinear loads into modern power systems poses significant challenges, primarily due to harmonic generation, which adversely affects power quality and grid stability. Harmonics in microgrids contribute to increased system losses, equipment overheating, and voltage distortions. To address this, implementing advanced energy management systems is crucial for reducing current harmonics to below 5% and voltage harmonics to below 8%, in accordance with standard limits [5]. Since fuel cells generate Direct Current (DC), appropriate power electronic converters and inverters are needed to convert it to Alternating Current (AC), ensuring effective and reliable integration into the microgrid infrastructure.

The Proportional-Integral Controller (PIC) is extensively utilized in EMS for power regulation; however, it encounters significant limitations under conditions characterized by weak grids and nonlinear load scenarios [6]. While Proportional-Integral (PI) controllers effectively regulate the DC-link voltage and fundamental current, they struggle to manage higher-order harmonics, exhibit sluggish transient response, and may incur overshoot and steady-state errors. These limitations adversely affect overall power quality in practical

doi: 10.18178/ijeetc.15.2.86-98

applications. To address these issues, recent research has developed many advanced EMS coupled with optimized controllers.

Amini, Rastegar, and Pichan [7] proposed an EMS employing a Proportional-Resonant (PR) controller, optimized through a Genetic Algorithm (GA). This controller can significantly minimize grid-side harmonics in utility systems, reducing the Total Harmonic Distortion (THD) from 20.2% to 4.2% for Resistive-Inductive (R-L) loads and from 56.1% to 4.5% for Resistive-Capacitive (R-C) loads. Despite their enhanced performance in harmonic compensation, PR controllers still struggle to eliminate low-order harmonics and cannot regulate the DC-link voltage as quickly as other, more advanced controllers. Another advanced control strategy in [8], developed a hybrid PI-PR control. This methodology maintains lower THD in the injected currents even under abnormal grid conditions while providing faster response times, diminished overshoot, shorter settling periods, and reduced steady-state errors. Chen *et al*. [9] proposed PR EMS achieving low THD, though weak grid and harmonic issues remain. Kumar *et al*. [10] introduced the Multipurpose and Power Quality Improved (MPQI) controller with a THD of 1.7%, but it relies on conventional converter and lacks validation in weak grids. Zhang *et al*. [11] developed a Particle Swarm Optimization (PSO) optimization-based controller that reduces THD from 23.90% to 4.01% for balanced loads. However, its implementation is challenging as convergence to local optima inherent to PSO algorithms. Li *et al*. [12] has developed an EMS based on a vector-proportion approach, which focuses only on nominal operating conditions, and lacks in evaluating under weak grid conditions, such as imbalances and high THD. Yilmaz and Turksoy [13] propose an AI-driven approach for reducing THD to under 2% in single-phase fuel cell systems, but requires long training and computationally complex and expensive controller. Additionally, a virtual vector-based Model Predictive Controller (MPC) algorithm study in [14], to enhance power quality in grid-connected PEMFC systems. However, this system places higher computational demands and introduces significant voltage ripples at the converter's output. Juan *et al*. [15] propose an adaptive DC-link method using MPC, proportional control, and a real-time observer, improving load performance but limited by weak grid issues, complexity, and the absence of harmonic compensation during severe disturbances. Al-Ani *et al*. [16] have developed an ANN-based new EMS for grid-connected hybrid renewable systems, but it excludes stability analysis and weak grid considerations. Bakria *et al*. [17] have proposed a Golden Jackal Optimizer (GJO)-based design of an EMS with optimized PI DC-link control and output filtering to enhance power quality. Their results show a significant reduction in grid-current THD from 14.64% to 0.8%. Nevertheless, GJO is prone to premature convergence and struggles with maintaining an effective balance between exploration and exploitation. Moreover, the benchmark is mainly against GA-based tuning; other recent advanced optimizers or adaptive controllers are not considered, which narrows the comparative perspective.

The literature review indicates that the fuel cell-integrated grid system mostly suffers from high THD, low energy conversion efficiency, lack of transient response, and power quality problems. Although some advanced control approaches, like the grid systems of [18, 19] were able to minimize the harmonics below the IEEE 519–2014 standard (i.e., <5%) the results were not highly satisfactory. A significant drawback in several of these studies is the dependence on a singular algorithm [11, 17]. This methodology may suffer from convergence to local optima, limited adaptability to changing conditions, and difficulty in addressing problem-specific insights. Besides that, most of these EMS were not tested during grid/load disturbances and transient loads, where the THD is particularly high. Therefore, considering this research gap, this paper proposed GBO based algorithm, inspired by Newtonian gradient search, to improve fuel cell power quality by balancing exploitation and reducing harmonics and THD in grid-connected systems. This paper offers original and significant contributions to the field, as summarized:

- The study introduces a GBO algorithm aimed at improving the transient response of the DC link voltage.
- The application of the GBO algorithm for the optimal tuning of control parameters has led to a significant reduction in THD and enhanced performance of the fuel cell integrated grid system.
- A comprehensive performance evaluation of the GBO algorithm was conducted using a rigorous assessment of the convergence characteristics of the grid-integrated fuel cell model.

## II. System Design and Implementation Steps

The proposed GBO controller and system topology are presented in Fig. 1, with the system design and implementation analyzed in the following sections. This part of the study has revealed the modeling of the energy source of PEMFC, examining its equivalent circuit, designing the DC-DC boost converter, determining the boost converter parameters, and developing two closed-loop control approaches to control the dc link voltage.

### *A. Energy Source (PEMFC)*

The PEMFCs generate electrical energy through an electrochemical reaction, utilizing hydrogen or natural gas as the fuel and oxygen from ambient air as the oxidant. This process yields DC electricity, accompanied by water and heat as by-products [20]. The equivalent circuit model of the PEMFC is illustrated in Fig. 2 [21]. The mathematical expression describing the output voltage of the fuel cell stack, as in Eq. (1):

$$V_{\mathrm{FC}} = N_{\mathrm{Cell}} \times E_{\mathrm{Cell}} = E - V_{\mathrm{Act}} - V_{\mathrm{Conc}} - V_{\mathrm{Ohmic}} \quad (1)$$

where, $N_{\mathrm{Cell}}$ refers to the number of individual fuel cells connected in series within the stack, $E_{\mathrm{Cell}}$ represents to voltage of a single fuel cell, $V_{\mathrm{FC}}$ shows the output voltage of the fuel cell, while $E$ represents the open circuit voltage, and $V_{\mathrm{Act}}$ , $V_{\mathrm{Conc}}$ and $V_{\mathrm{Ohmic}}$ provide the activation, concentration, and ohmic voltages of the fuel cell, correspondingly. In addition, the relationship between

voltage and current for fuel cell stacks can be modeled as follows, as in Eq. (2):

$$V_{\mathrm{FC}} = E - AT\ln\left(\frac{I_{\mathrm{FC}}}{I_o}\right) - BT\ln\left(\frac{I_L - I_{\mathrm{FC}}}{I_L}\right) - I_{\mathrm{FC}}\,R_{\mathrm{int}} \quad (2)$$

where $T$ represents the operating temperature of the fuel cell, $I_{\mathrm{FC}}$ indicates the current produced by the fuel cell, $I_o$ change current, $I_L$ limit current, $R_{\mathrm{int}}$ represents the internal resistance, $A$ is the activation coefficient, and $B$ is the concentration coefficient.

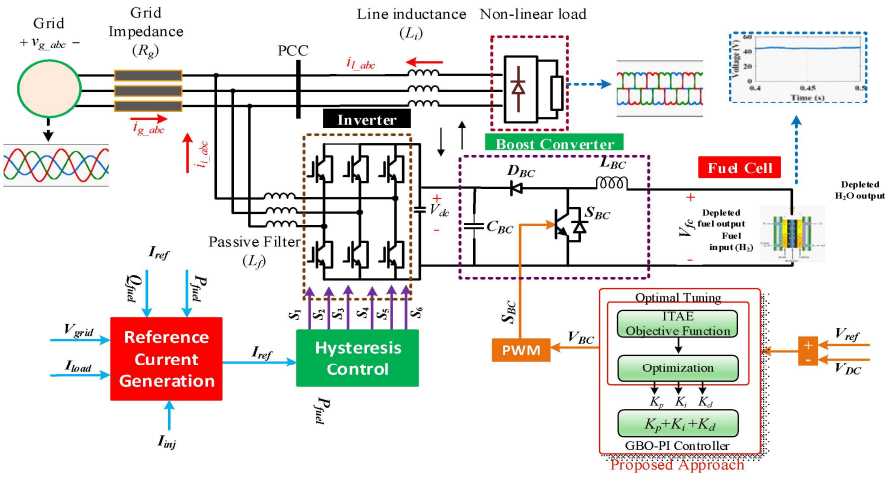


Fig. 1. Proposed GBO controller and system topology.

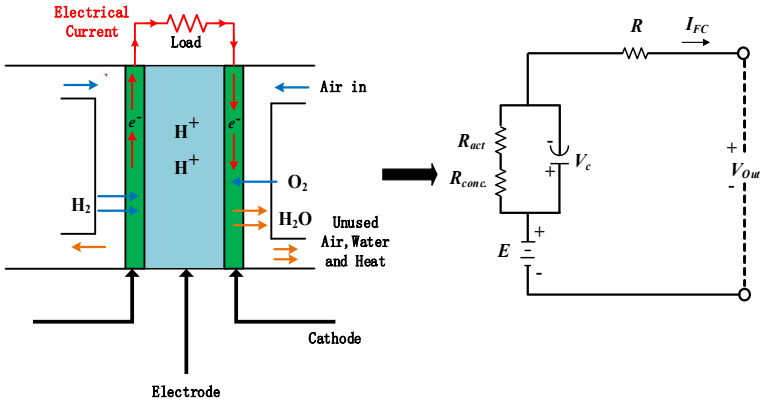


Fig. 2. Representing the equivalent circuit of the PEM fuel cell.

The characteristic curves depicting the current-voltage and current-power relationships of the 6 kW PEM fuel cell utilized in this research are illustrated in Fig. 3.

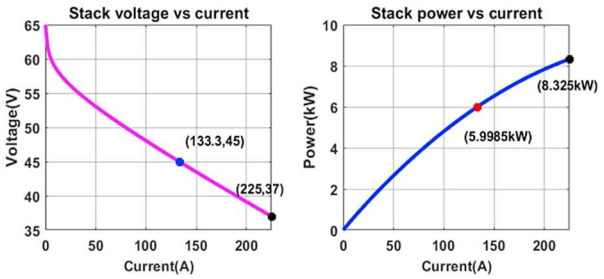


Fig. 3. The current-voltage and current-power relationships of the 6 kW PEM fuel cell.

## B. DC-Link Control

A DC–DC boost converter is employed to step up the voltage output from the PEM fuel cell prior to supplying it to the single-phase full-bridge inverter. The boost converter is selected in this study owing to its simple structure, ease of implementation, compact design, and reliable power transfer capability. Furthermore, a PIC is utilized to regulate the boost converter, ensuring that the output voltage tracks a predefined reference value [22]. The mathematical expression for the output voltage of the boost converter is given in Eq. (3).

$$V_{\mathrm{dc}} = \frac{V_F}{1-D} \quad (3)$$

where $V_{\mathrm{dc}}$ represents the output voltage of the boost converter, $D$ indicates the duty cycle and $V_F$ indicates the fuel cell voltage. The minimum value of the inductor, $L_{\mathrm{BC}}$ is calculated as

$$L_{\mathrm{BC\,(min)}} = \frac{D(1-D)^2 R}{2f} \quad (4)$$

where $R$ refers to the load resistance, and $f$ represents the switching frequency. The value of the capacitor, $C_{\mathrm{BC}}$ is determined by

$$C_{\mathrm{BC}} = \frac{D}{R\left(\frac{\Delta V_{\mathrm{dc}}}{V_{\mathrm{dc}}}\right)f} \quad (5)$$

where $\Delta V_{\mathrm{dc}}$ is the ripple voltage of the boost converter.

### C. Proposed Controller Design

This section introduces an efficient switching strategy designed to stabilize the system and achieve the desired output in the presence of load disturbances and unmodeled dynamics. The average state-space Linear Time-Invariant (LTI) representation of the converter exhibits significant sensitivity to variations in input voltage, load fluctuations, external disturbances, modelling uncertainties, and sensor inaccuracies. To address these challenges, a robust GBO-based PI tuning controller is proposed, which regulates the duty cycle ($u$) of the boost converter switch to track the optimal reference voltage ($V_{\mathrm{cref}}$).

### D. PI Controller Design

The proposed control mechanism employs a GBO-optimized PIC, referred to as GBO-PIC, which is primarily responsible for regulating the output of the boost converter. The objective of this controller is to minimize the tracking error by comparing the actual output with the desired reference value, as formulated in Eq. (6). For comparative evaluation, the controller is expressed in Eq. (7), where the proportional $K_p$ and integral $K_i$ gains of the PI controller are optimally tuned using the GBO algorithm.

$$u(t) = 1 - U_{\mathrm{pi}} \tag{6}$$

$$U_{\mathrm{pi}} = K_p(V_{\mathrm{cref}} - V_c) + K_i f(V_{\mathrm{cref}} - V_c)dt \tag{7}$$

where $u(t)$ refers to the control signal or duty cycle command applied to the converter's switch, $V_c$ refers to the actual (measured) output voltage of the converter and $U_{\mathrm{pi}}$ refers to the output of the PI controller, which adjusts based on the error between $V_{\mathrm{ref}}$ and $V_c$.

### E. Proposed Control Methodology

Single-phase full-bridge inverters represent a fundamental topology in power electronics owing to their simple design and bidirectional power-flow capability. In this configuration, the energy generated by the fuel cell is converted from DC to AC form for grid integration. In the present study, the switching signals of the single-phase full-bridge inverter are modulated to enable precise control of both active and reactive power. The grid voltage serves as the reference for phase angle synchronization, which is achieved through a Phase-Locked Loop (PLL) control mechanism.

The $d$–$q$ transformation converts the reference AC waveforms into DC quantities, thereby eliminating the influence of time-dependent components. These DC signals facilitate simplified computational processing, after which an inverse transformation is applied to reconstruct the corresponding AC signals. The mathematical formulation of the $d$–$q$ transformation in matrix form is presented in (8). Depending on the application, the variable $\mathbf{X}$= $[\mathbf{X}_d \quad \mathbf{X}_q]^T$ may represent either voltage or current [23].

$$\begin{bmatrix}\mathbf{X}_d\\ \mathbf{X}_q\end{bmatrix} = \begin{bmatrix}\sin(\omega t) & -\cos(\omega t)\\ \cos(\omega t) & \sin(\omega t)\end{bmatrix}\begin{bmatrix}\mathbf{X}_\alpha\\ \mathbf{X}_\beta\end{bmatrix} \tag{8}$$

where $t$ is the time and hence, $T$ simply indicates the transpose operation, ensuring the vector has the correct orientation for matrix multiplication in the $d$–$q$ transformation. $\mathbf{X}_d$, $\mathbf{X}_q$, $\mathbf{X}_\alpha$, and $\mathbf{X}_\beta$ represent the $d$-axis, $q$-axis, $\alpha$-axis and $\beta$-axis components, respectively. The symbol $\omega$ represents the angular frequency of the rotating reference frame.

Park's Eq. (9) to (11) describe the dynamic behavior of current and voltage, incorporating the angular frequency ($\omega_o$), which rotates synchronously with the inverter output voltage.

$$\left.\begin{aligned}\frac{di_{\mathrm{id}}}{dt} &= -\frac{R_f}{L_f}i_d + \omega_o i_{\mathrm{qL}} + \frac{1}{L_f}(v_{\mathrm{id}} - v_{\mathrm{dc}})\\ \frac{di_{\mathrm{qL}}}{dt} &= -\frac{R_f}{L_f}i_q + \omega_o i_{\mathrm{dL}} + \frac{1}{L_f}(v_{\mathrm{iq}} - v_{\mathrm{qc}})\end{aligned}\right\} \tag{9}$$

$$\left.\begin{aligned}\frac{dv_{\mathrm{id}}}{dt} &= \omega_o v_{\mathrm{qc}} + \frac{1}{C_f}(i_{\mathrm{id}} - i_{\mathrm{dL}})\\ \frac{dv_{\mathrm{qc}}}{dt} &= -\omega_o v_{\mathrm{dc}} + \frac{1}{C_f}(i_{\mathrm{iq}} - i_{\mathrm{qL}})\end{aligned}\right\} \tag{10}$$

$$\left.\begin{aligned}\frac{di_{\mathrm{dL}}}{dt} &= -\frac{R_g}{L_g}i_{\mathrm{dL}} + \omega_o i_{\mathrm{qL}} + \frac{1}{L_f}(v_{\mathrm{dc}} - v_{\mathrm{dL}})\\ \frac{di_{\mathrm{qL}}}{dt} &= -\frac{R_g}{L_g}i_{\mathrm{qL}} - \omega_o i_{\mathrm{dL}} + \frac{1}{L_f}(v_{\mathrm{qc}} - v_{\mathrm{qL}})\end{aligned}\right\} \tag{11}$$

where $R_f$ filter inductor resistance, $L_f$ filter inductance, $R_g$ grid-side inductor resistance, and $L_g$ grid-side inductance. The output voltages and currents of the d-axis and q-axis are represented by $v_{\mathrm{dc}}$, $v_{\mathrm{qc}}$, $i_{\mathrm{dL}}$, and $i_{\mathrm{qL}}$ in the preceding equations, whereas the voltages and currents of the d-axis and q-axis inverters are represented by $v_{\mathrm{id}}$,$v_{\mathrm{iq}}$, $i_{\mathrm{id}}$ and $i_{\mathrm{iq}}$.

## III. Gradient-Based Optimization (GBO) Algorithm

Although PSO, Harris Hawks Optimization (HHO), and GJO possess notable strengths, they also exhibit certain drawbacks, especially the premature convergence and getting trapped in local optima. As a result, the proposed approach called GBO, is introduced. It is expected to improve convergence behaviour and solution quality. The GBO algorithm integrates gradient and population-based approaches to determine the search direction. This is achieved by applying Newton's method to explore the search domain using a collection of vectors and two primary operators, the gradient search rule and local escaping operators. The optimization challenges include minimizing the objective function.

*Initialization*: An optimization problem consists of a collection of decision variables, constraints, and an objective function. The control parameters of the GBO consist of a transition parameter that determines the shift from exploration to exploitation ($\beta$) and a probability rate. The number of iterations and the population size are determined by the task's difficulty. Everyone in the proposed method is referred to as a 'vector' inside the population.

The GBO consists of $\mathbf{M}$ vectors within a search space of $D$-dimensions. Therefore, a vector can be represented as:

$$\mathbf{Y}_{m,d} = \left[\mathbf{Y}_{m,1}, \mathbf{Y}_{m,1}, \cdots, \mathbf{Y}_{m,D}\right] \quad m = 1, 2, \ldots, \mathbf{M}, d = 1, 2, \ldots, D \tag{12}$$

Typically, the GBO's initial vectors are randomly generated inside the D-dimensional search domain, which is specified as:

$$\mathbf{Y}_m = \mathbf{Y}_{\min} + p(0,1) \times (\mathbf{Y}_{\max} - \mathbf{Y}_{\min}) \tag{13}$$

where the values of $\mathbf{Y}_{\min}$ and $\mathbf{Y}_{\max}$ represent the lower and upper limits, respectively, of the decision variable $\mathbf{Y}$. The term $p(0, 1)$ refers to a random number that falls within the range of [0, 1].

Gradient Search Rule (GSR): The gradient search rule regulates the movement of vectors to enhance exploration within the feasible domain and attain optimal placements. The GSR is proposed to enhance exploration and accelerate convergence of the GBO by leveraging the GB technique. Nevertheless, this rule is derived from Newton's gradient-based technique [24]. Due to the non-differentiability of many optimization problems, a numerical gradient approach is used as an alternative to directly calculating the function's derivative. The GB technique typically starts with an estimated starting solution and iteratively progresses towards the next position in a direction determined by the gradient. To obtain the GSR using Eq. (14), it is necessary to compute the first-order derivative using the Taylor series. The Taylor series expansions for both functions $F(y + \Delta y)$ and $F(y - \Delta y)$ can be stated as follows:

$$F(y + \Delta y) = F(y) + F'(y_0)\Delta y + \frac{F''(y_0)\Delta y^2}{2!} + \frac{F'''(y_0)\Delta y^3}{3!} + \cdots \tag{14}$$

$$F(y - \Delta y) = F(y) - F'(y_0)\Delta y + \frac{F''(y_0)\Delta y^2}{2!} - \frac{F'''(y_0)\Delta y^3}{3!} + \cdots \tag{15}$$

Here, the value of the function $F$ at point $y$, the value of the function at a point slightly shifted from $y$ by a small increment $\Delta y$, and $y_0$, is the point around which the Taylor series is expanded.

The first-order derivative can be obtained using the central differencing formula in [25].

$$F'(y) = \frac{F(y+\Delta y) - F(y-\Delta y)}{2\Delta y} \tag{16}$$

The new position $(x_n + 1)$ is defined based on Eq. (14) and Eq. (16):

$$y_{n+1} = y_n - \frac{2\Delta y F(y_n)}{F(y_n+\Delta y) - F(y_n-\Delta y)} \tag{17}$$

Given that the GSR is regarded as the central component of the proposed method, several adjustments are necessary to manage the population-based search effectively. Concerning Eq. (17), the adjacent positions of $y$ are $(y + \Delta y)$ and $(y_n - \Delta y)$. In the GBO method, these adjacent positions are substituted with two alternative positions (vectors) in the population. In the minimization problem, the position has a lower fitness than $y_n$, however $y_n - \Delta y$ has a higher fitness than $y_n$. The GBO algorithm replaces the position with a better location in the neighborhood of position $y_n - \Delta y$, and replaces with $y_{\text{best}}$, which is a worse position in the neighborhood of $y_n$. Furthermore, the suggested technique utilizes the position $(y_n)$ rather than its fitness $F(y_n)$ due to the increased computational cost associated with using the fitness of a location. The proposed GSR is formulated in the following manner:

$$\text{GSR} = \text{pn} \times \frac{2\Delta y y_n}{(y_{\text{worst}} - y_{\text{best}} + \epsilon)} \tag{18}$$

Here, $pn$ is a normally distributed random number, $\epsilon$ is a tiny number that falls between the range of 0 and 0.1. $y_{\text{best}}$ and $y_{\text{wrost}}$ represent the optimal and suboptimal solutions achieved throughout the optimization procedure, respectively.

Eq. (18) can aid the current solution in updating its position. To enhance the search functionality of the proposed GBO algorithm and achieve a balance between global exploration and local exploitation, the GSR is adjusted by incorporating a random parameter $\wp_1$ in Eq. (18), as explained in the following manner.

$$\wp_1 = (2p\beta) - \beta \tag{19}$$

$$A = \left|\beta \sin\left(\frac{3\pi}{2} + \sin\left(\beta \frac{3\pi}{2}\right)\right)\right| \tag{20}$$

$$\beta = \beta_{\min} + (\beta_{\max} - \beta_{\min})\left(1 - \left(\frac{n}{\mathcal{M}}\right)^3\right)^2 \tag{21}$$

where the values of $\beta_{\min}$ and $\beta_{\max}$ are 0.2 and 1.2, respectively. $\mathcal{M}$ represents the total number of iterations, while the variable $n$ represents the number of iterations. To maintain a balance between exploration and exploitation, parameter $\wp_1$ is adjusted based on the sine function. The maximum iteration number is set at 1000. The parameter can be modified at each iteration, starting with high value to promote population diversity in the early iterations and gradually decreasing as the iteration number increases to expedite convergence. The solutions created should be able to systematically investigate the search space surrounding their respective optimal solutions. The parameter value increases between iterations 550 and 750, helping the proposed method avoid local optima by increasing the diversity of the population's search for the best solution. Hence, Eq. (18) can be restated as:

$$\text{GSR} = \text{pn} \times \wp_1 \frac{2\Delta y y_n}{(y_{\text{worst}} - y_{\text{best}} + \epsilon)} \tag{22}$$

The suggested solution enables the GBO to effectively consider unpredictable behavior throughout the optimization process, facilitating exploration and avoiding getting stuck in local optima. In Eq. (22), the value of $\Delta y$ is calculated by subtracting the best solution $y_{\text{best}}$ from a randomly chosen position $y_{w1}^n$ (as described in Eq. (23), Eq. (24), and Eq. (25). To guarantee that $\Delta y$ varies with each iteration, the parameter $\delta$ is determined using Eq. (14). An additional random number $P$ is incorporated into Eq. (14) to enhance exploration.

$$\Delta y = p(1{:}N) \times |\text{step}| \tag{23}$$

$$\text{step} = \frac{(y_{\text{best}} - y_{w1}^n) + \delta}{2} \tag{24}$$

$$\delta = 2 \times p\left(\left|\frac{y_{w1}^n + y_{w2}^n + y_{w3}^n + y_{w4}^n}{4} - y_n^m\right|\right) \quad (25)$$

where the expression $p(1{:}N)$ generates a random number with $N$ dimensions. The variables $w_1$, $w_2$, $w_3$, and $w_4$ ($w_1 \neq w_2 \neq w_3 \neq w_4 \neq n$) are distinct integers randomly selected from the range [1, $N$]. The step size, denoted as step, is determined by the values of $y_{\text{best}}$ and $y_{w1}^n$. By utilizing the proposed GSR, Eq. (23) can be reformulated as follows:

$$y_{n+1} = y_n - \text{GSR} \quad (26)$$

The inclusion of the direction of movement (DM) is implemented to utilize the surrounding vicinity of the specified location more effectively. This term utilizes the optimal vector and displaces the current vector, $y_n$ towards the direction of $y_{\text{best}} - y_n$. Thus, this procedure generates a favorable inclination for local exploration, which enhances the rate at which the GBO algorithm converges. The proposed DM model is expressed in the following manner:

$$\text{DM} = p \times \wp_2(y_{\text{best}} - y_n) \quad (27)$$

where $\wp_2$ is a randomly generated parameter that helps each vector have a distinct step size.

Furthermore, this can serve as an additional element of the GBO that bolsters the process of investigation. The value of $\wp_2$ is determined by:

$$\wp_2 = 2p\beta - \beta \quad (28)$$

Finally, the position of the current vector ($y_m^n$) can be updated using Eq. (29) and Eq. (30) according to the terms of the GSR and DM.

$$Y_{1n}^m = y_n^m - \text{GSR} + \text{DM} \quad (29)$$

$$Y_{1n}^m = y_n^m - \left\{p\wp_1 \frac{2\Delta y \times y_n^m}{(y_{\text{worst}} - y_{\text{best}} + \epsilon)}\right\} + p\wp_2(y_{\text{best}} - y_n^m) \quad (30)$$

where $Y_{1n}^m$ is the resultant vector obtained after updating $y_n^m$.

Fig. 4 illustrates that the position $Y_{1n}^m$ is generated at a randomly selected point in the search space, as determined by the GSR and DM. The study utilizes Özban's Newton's approach Eq. (11) to enhance the GSR [26]. The GSR can be represented as a function of Eq. (17) and Eq. (22).

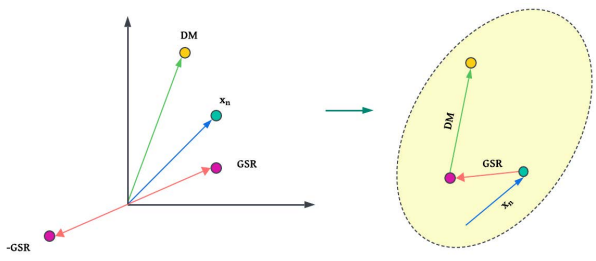


Fig. 4. The process of updating the current position.

The position of the present solution can be modified by using a formula distinct from Eq. (23) as

$$y_{n+1} = y_n - \frac{2\Delta y \times f(y_n)}{f(x_n + \Delta y) - f(x_n - \Delta y)} \quad (31)$$

Here

$$x_n = \frac{|q_{n+1} + y_n|}{2} \quad (32)$$

This equation utilizes the mean of two vectors, $q_{n+1}$ and $y_n$, rather than just one. This novel formula can enhance the optimization method by refining the search process within the solution space. Like Eq. (26), to transform Eq. (33) into a search strategy based on population, the variable $q_{n+1}$ is initially defined as:

$$q_{n+1} = y_n - \frac{2\Delta y \times f(y_n)}{f(y_n + \Delta y) - f(y_n - \Delta y)} \quad (33)$$

Next, to transition to a population-based method, Eq. (33) can be reformulated as:

$$q_{n+1} = y_n - \left\{\text{pn} \times \frac{2\Delta y y_n}{(y_{\text{worst}} - y_{\text{best}} + \epsilon)}\right\} \quad (34)$$

The values of $(y_n + \Delta y)$ and $(y_n - \Delta y)$ in Eq. (20) are provided, as follows:

$$xa_n = p\left(\frac{[q_{n+1} + y_n]}{2} + p\Delta y\right) \quad (35)$$

$$xb_n = p\left(\frac{[q_{n+1} + y_n]}{2} - p\Delta y\right) \quad (36)$$

Here, $xa_n$ and $xb_n$ are two positions relative to $q_{n+1}$ and $y_n$, respectively. By utilizing the aforementioned equations, the GSR can be formulated as:

$$\text{GSR} = \text{pn} \times \wp_1 \times \frac{2\Delta y y_n}{(xa_n - xb_n + \epsilon)} \quad (37)$$

Eq. (38) and Eq. (39) are utilized to determine the position of $Y_{1n}^m$ in relation to the GSR and DM.

$$Y_{1n}^m = y_n^m - \text{GSR} + \text{DM} \quad (38)$$

By substituting the current vector ($y_{\text{best}}$) for the location of the best vector ($y_n^m$) in Eq. (36), we can produce the new vector ($Y_{2n}^m$) using the following method:

$$Y_{1n}^m = y_{\text{best}} - \left\{\text{rand}n \times \wp_1 \frac{2\Delta y \times y_n}{(xa_n^m - xb_n^m + \epsilon)}\right\} + \{p \times \wp_2(y_{r1}^m - y_{r2}^m)\} \quad (39)$$

This search strategy prioritizes the process of using available resources. The search strategy described in Eq. (39), which is effective for local search but has limitations for global search. Conversely, the search method presented in Eq. (39) is effective for global search but has limitations for local search. Thus, the GBO utilizes both search strategies in Eq. (38) and Eq. (39) to improve both exploration and exploitation. Therefore, using the coordinates $Y_{1n}^m$, $Y_{2n}^m$, and the current position ($Y_n^m$), the new solution at the following iteration ($Y_n^{m+1}$) may be precisely stated as:

$$y_n^{m+1} = w_a\{w_b Y_{1n}^m + (1 - w_b)Y_{2n}^m\} + (1 - w_b)Y_{3n}^m \quad (40)$$

$$Y_{3n}^m = Y_n^m - \{\wp_1(Y_{2n}^m - Y_{1n}^m)\} \quad (41)$$

where $w_a$ and $w_b$ are two random numbers chosen from the interval [0, 1].

Fig. 5 illustrates the process by which a vector adjusts its location relative to $Y_{1n}^m$, $Y_{2n}^m$, and $Y_{3n}^m$ in a two-dimensional search space. Based on Fig. 5 and Eq. (40), the position in the search space would be selected randomly by the positions $Y_{1n}^m$, $Y_{2n}^m$, and $Y_{3n}^m$. These three

places specifically define the position $y_n^{m+1}$, while other vectors undergo random positional changes relative to $y_n^{m+1}$.

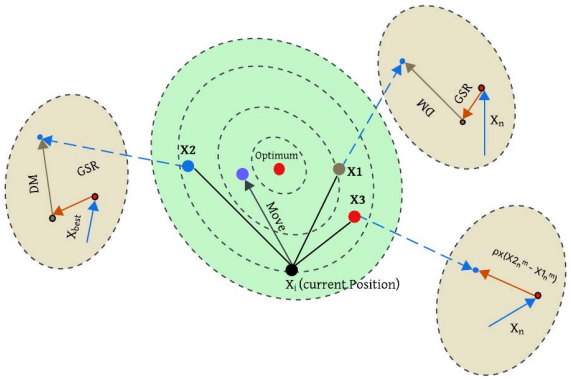


Fig. 5. Conceptual diagram of the GBO algorithm.

Local Escaping Operator (LEO): The LEO is implemented to enhance the effectiveness of the suggested GBO algorithm in resolving intricate situations. This operator can substantially alter the position of the solution $y_n^{m+1}$. The LEO algorithm produces a high-performing solution $y_{\text{LEO}}^m$ by combining multiple solutions, such as the best position ($y_{best}$), solutions $Y_{1n}^m$ and $Y_{2n}^m$, two random solutions $y_{w1}^m$ and $y_{w2}^m$, and a newly created solution ($y_k^m$). The answer $y_{\text{LEO}}^m$ is derived using the following scheme:

If $p < \wp w$

if $p < 0.5$

$$Y_{\text{LEO}}^m = Y_n^{m+1} + F_1(v_1 y_{\text{best}} - v_2 y_k^m) + F_2 \wp_1 \left(v_3 (Y_{2n}^m - Y_{1n}^m) + v_2 (y_{w1}^m - y_{w2}^m)\right)/2 \quad (42)$$

Else

$$Y_{\text{LEO}}^m = Y_n^{m+1} + F_1(v_1 y_{\text{best}} - v_2 y_k^m) + F_2 \wp_1 \left(v_3 (Y_{2n}^m - Y_{1n}^m) + v_2 (y_{w1}^m - y_{w2}^m)\right)/2$$

$$Y_n^{m+1} = Y_{\text{LEO}}^m$$

End

end

Here, the variable $F_1$ is a random number that is uniformly distributed between –1 and 1. The variable $F_2$ is a random number that follows a normal distribution with a mean of 0 and a standard deviation of 1. The probability is denoted by this variable. $w$ random numbers chosen from the interval [0, 1]. The variables $v_1$, $v_2$, and $v_3$ are three random numbers that are defined as:

$$v_1 = \begin{cases} 2p & \text{if } \mu_1 < 0.5 \\ 1 & \text{otherwsie} \end{cases} \quad (43)$$

$$v_2 = \begin{cases} p & \text{if } \mu_1 < 0.5 \\ 1 & \text{otherwsie} \end{cases} \quad (44)$$

$$v_3 = \begin{cases} p & \text{if } \mu_1 < 0.5 \\ 1 & \text{otherwsie} \end{cases} \quad (45)$$

Here, $\mu_1$ represents any number between 0 and 1. The equations mentioned earlier can be further simplified:

$$v_1 = 2S_1 p + (1 - S_1) \quad (46)$$

$$v_2 = S_1 p + (1 - S_1) \quad (47)$$

$$v_3 = S_1 p + (1 - S_1) \quad (48)$$

where parameter $S_1$ is a binary variable that can take on a value of either 0 or 1. If the parameter $v_1$ is below 0.5, the value of $S_1$ is set to 1; otherwise, it is set to 0. To find the solution $y_k^m$ in (42), the suggested approach is as follows.

$$y_k^m = \begin{cases} y_p & \text{if } \mu_2 < 0.5 \\ y_\wp^m & \text{otherwise} \end{cases} \quad (49)$$

$$y_p = Y_{\min} + p(0,1) \times (Y_{\max} - Y_{\min}) \quad (50)$$

Here, $y_p$ is a new solution, $y_\wp^m$ represents a solution randomly chosen from the population (where $\wp$ belongs to the range [1, 2, ···, $N$]), and $\mu_2$ is a random value within the range of [0, 1]. Equation (39) can be simplified as follows:

$$y_k^m = S_2 y_\wp^m + (1 - S_2) y_p \quad (51)$$

where parameter $S_2$ is a binary variable that can only take the values of 0 or 1.

If the value of $v_2$ is less than 0.5, then the value of $S_2$ is assigned as 1. Otherwise, it is assigned as 0. The stochastic selection of values for parameters $v_1$, $v_2$, and $v_3$ promotes population diversity and helps avoid being trapped in local optimal solutions.

The pseudo-code of the GBO algorithm outlines the systematic procedure employed to determine the optimal controller parameters for the fuel cell grid-integrated system, is displayed in Algorithm 1. Through iterative evaluation and updating of the best and worst solutions, the algorithm effectively minimizes objective functions such as total harmonic distortion, settling time, and overshoot, thereby enhancing overall system performance. The incorporation of random selection and a local escaping operator prevents premature convergence, ensuring global optimality and robust controller tuning. Consequently, the final optimal solution obtained ($y_{\text{best}}^m$) enables precise voltage regulation, faster transient response, and improved grid stability. This optimization process ensures efficient and reliable operation of the fuel cell-based grid-connected system under varying load and disturbance conditions.

Algorithm 1: Pseudo-code of the GBO algorithm

Step 1: Initialization

Assign values for parameters $\wp$w, $\varepsilon$, $\mathcal{M}$

Generate an initial population $Y_0 = [y_{0,1}, y_{0,2}, \cdots, y_{0,D}]$

Evaluate the objective function value $F(Y_0), n = 1, \ldots, N$

Specify the best and worst solutions $y_{\text{best}}^m$ and $y_{\text{worst}}^m$

Step 2: Main loop

While ($m < \mathcal{M}$)

For $n$ = 1:$N$

For $i$ = 1:$D$

Select randomly $w_1 \neq w_2 \neq w_3 \neq w_4 \neq n$ in the range of [1, $N$]

Calculate the position $y_{n,i}^{m+1}$ using (40)

end for

Local escaping operator

if $p < \wp$w

Calculate the position $y_{\text{LEO}}^m$ using (42)

$Y_n^{m+1} = y_{\text{LEO}}^m$

end

Update the position $y_{\text{best}}^m$ and $y_{\text{worst}}^m$

end for

$m = m + 1$

end

Step 3: return $y_{\text{best}}^m$

The parameter settings presented in Table I play a vital role in ensuring effective optimization performance for the fuel cell-based grid-integrated system. Each parameter governs the balance between exploration and exploitation, influencing the convergence speed and solution accuracy of the respective algorithms. Proper tuning of these parameters, such as the escaping energy ($r$) in HHO, the control parameter ($\alpha$) in GBO, and the inertia factor in PSO enables robust adaptation to dynamic operating conditions.

This careful parameter configuration ensures optimal controller tuning, resulting in improved transient response, reduced total harmonic distortion, and enhanced overall stability of the grid-connected fuel cell system. After that, the main flowchart of the GBO-based algorithm is presented in Fig. 6, along with a simplified flowchart in Fig. 7.

TABLE I: SETTING OF ALGORITHM PARAMETERS

| Algorithm | Parameters | Value |
|---|---|---|
| HHO | Default constant, $\beta$ | 1.5 |
| | Random number, $r_1$ | [0, 1] |
| | Escaping energy, $E$ | [0 1] |
| | Initial energy, $E_0$ | [−1 1] |
| GJO | Prey Energy, $E_1$ | [1.5, 0] |
| PSO | Factor of inertia | 0.3 |
| | Acceleration coefficients, $c1$ | 1 |
| | Acceleration coefficients, $c2$ | 1 |
| GBO | Control parameter, $\alpha$ | [0, 1] |
| | Local escaping operator (LEO) probability | 0.5 |
| | Transition parameter, $\beta$ | [0, 1] |
| | Epsilon, $\epsilon$ | [0, 1] |

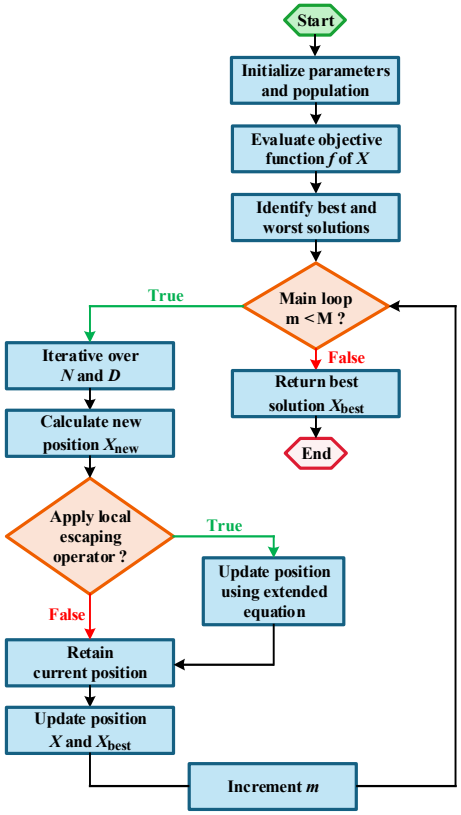


Fig. 6. Flowchart of the GBO-based algorithm.

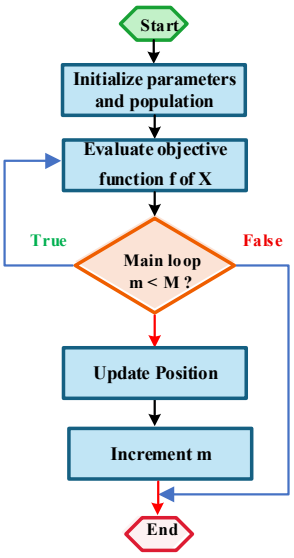


Fig. 7. Simplified flowchart of the GBO-based algorithm.

## IV. SIMULATION RESULTS

This section validates the performance of the proposed HO-HHO-PI controller through a series of simulation results, where the simulation is carried out using MATLAB Simulink, and the performance evaluation is undertaken under three distinct scenarios representing prevalent grid disturbances encountered in the fuel cell integrated grid system. These scenarios are carefully selected to cover a range of common disturbances. The harmonic distortion of the grid-connected fuel cell has been evaluated via three case scenarios: Case 1: fixed 880V DC link voltage, Case and Case 2: DC link voltages ranging from 1000V to 700V.

### *A. Case Study 1: Fixed 880V DC Link Voltage (Non-Linear Load)*

This section analyzes case study 1 at a fixed 880V to observe the THD of the grid currents and the transient response. The conventional algorithm has a THD of 6.61% for grid currents in Fig. 8 (a), whereas the proposed algorithm significantly improves performance with a THD of only 0.60%, as observed in Fig. 8 (b). The proposed GBO-PI algorithm achieves a grid current THD of 0.60%, representing an absolute reduction of 6.01 percentage points and a 90.92% improvement compared to the conventional method (6.61%). This substantial reduction confirms the superior harmonic suppression capability of the GBO-PI–based control strategy.

Reducing the THD in a fuel cell grid-integrated system is vital to enhancing grid stability and power quality. A lower THD minimizes current and voltage distortions, thereby improving system efficiency and prolonging the lifespan of grid-connected components. It also mitigates overheating, resonance, and electromagnetic interference, contributing to smoother grid operation. Consequently, achieving low THD ensures compliance with IEEE 519 standards and significantly strengthens the overall stability and reliability of the power network.

The proposed controller exhibits the shortest settling time, equal to HHO, achieving a notable value of 0.022 s,

as shown in Fig. 9. This performance surpasses that of the no-controller scheme, which settles at 0.03 s, while GJO-PI and PSO-PI demonstrate longer settling times of 0.055 s and 0.057 s, respectively. Specifically, the GBO-PI controller improves the settling time by 61.4%, 60.0%, and 26.7% compared to PSO-PI, GJO-PI, and the no-controller case, respectively. A shorter settling time in a fuel cell grid-integrated system signifies a faster dynamic response and enhanced stability under load or voltage disturbances. The proposed GBO-PI controller enables the system to swiftly reach steady-state conditions, minimizing transient oscillations and power fluctuations. This improvement enhances grid synchronization, ensures smoother power delivery, and contributes to the overall reliability and operational efficiency of the grid-connected fuel cell system.

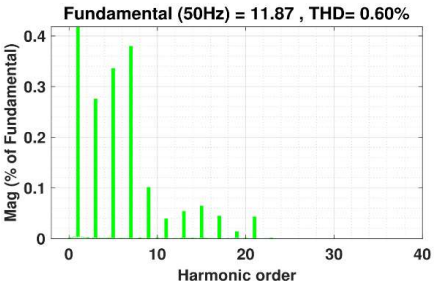


(a)

(b)

Fig. 8. Harmonic spectrums of (a) GBO-PI and (b) conventional controller under case study 1.

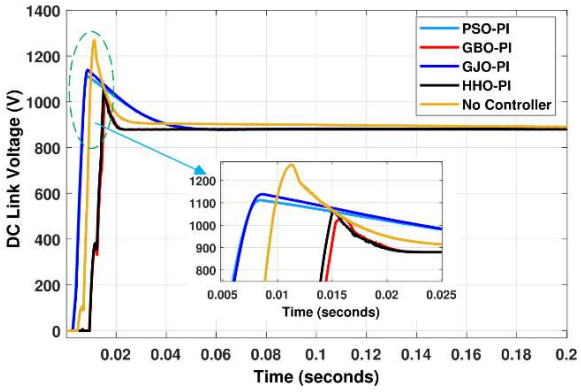


Fig. 9. A comparative analysis of DC link voltage response over time for different PI-based control strategies for fixed 880 V (case study 1).

The proposed GBO-PI achieves a maximum overshoot of 16.93%, representing 18.2%, 36.7%, and 42.4% relative reductions compared to HHO-PI (20.70%), PSO-PI (26.76%), and GJO-PI (29.40%), respectively. Compared with the worst-performing controller (44.20% overshoot), GBO-PI reduces overshoot by 61.6%. These reductions indicate a substantial improvement in transient damping achieved by GBO-PI in Fig. 9.

A lower overshoot in a fuel cell grid-integrated system indicates improved transient stability and precise control during dynamic conditions. The proposed GBO-PI controller effectively limits overshoot, reducing voltage and current deviations during disturbances. This makes it more effective for maintaining DC link voltage regulation in the grid-integrated fuel cell. This ensures smoother power delivery, enhanced grid stability, and protection of system components from stress and oscillations.

### *B. Case Study 2: (Non-Linear Load) Varying DC Link Voltage of 1000V to 700V*

The results indicate that the conventional algorithm yields a THD of 3.72% % for grid currents, outlined in Fig. 10 (a). In contrast, the proposed controller demonstrates a marked performance, achieving a THD of 0.82%, effectively complying with the IEEE 519 standard, as shown in Fig. 10 (b). The proposed GBO-PI controller achieves a grid-current THD of 0.82%, corresponding to an absolute reduction of 2.90 percentage-points and a 77.96% improvement compared to the conventional method (3.72%). This significant reduction not only highlights the enhanced harmonic mitigation capability of the GBO-PI strategy but also ensures compliance with the IEEE 519 standard.

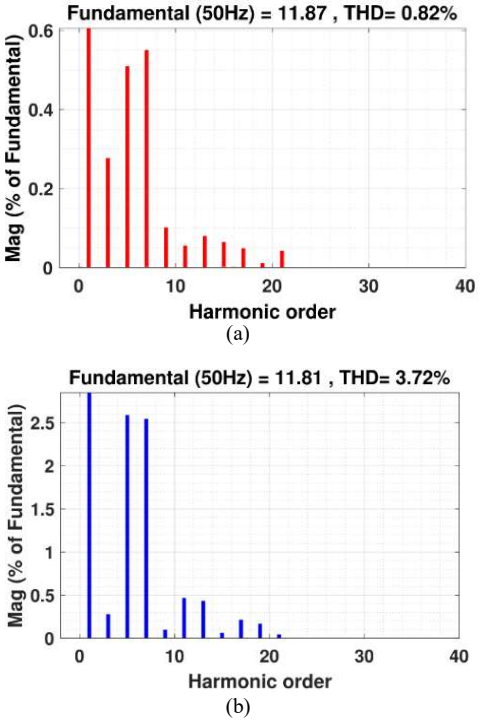


(a)

(b)

Fig. 10. Harmonic spectrums of (a) GBO-PI and (b) conventional controller under case study 2 (1000V to 700V).

When the DC-link voltage is held at 1000 V until 0.1 s, the system without a controller shows the highest overshoot ($O_p$) of 67.97%, followed by GJO-PI (48.22%) and HHO-PI (45.43%). The proposed GBO-PI achieves the lowest overshoot of 23.77%, outperforming them and

closely matches to PSO-PI (21.1%) but with reduced oscillations. Consequently, the proposed GBO-PI outperforms the compared methods by 34.21%, 14.46%, 11.67% for no controller, GJO-PI, and HHO-PI, respectively, in Fig. 11. The lower overshoot achieved by the proposed GBO-PI controller enhances transient stability and control precision in the fuel cell grid-integrated system. This improvement ensures smoother power transfer and greater protection of grid-connected components.

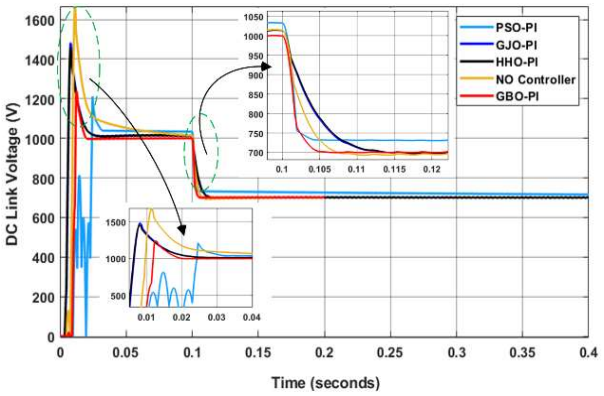


Fig. 11. The transient response of DC link voltage over time for different control strategies for 1000V to 700V (case study 2).

The proposed GBO achieves the fastest settling time of 0.020s, clearly outperforming all other controllers, represented in Fig. 11. Compared to PSO (0.032 s) and both GJO and HHO (0.030 s), it is around 33–37% faster, ensuring quicker stability. Against No controller (0.095 s), the proposed GBO shows a remarkable 78.9% improvement, highlighting its robustness, and most effective controller for rapid system stabilization. This reduced settling time of the proposed controller in fuel cell grid-integrated system reflects superior dynamic performance and improved stability under non-linear load conditions. The GBO-PI controller demonstrates improved performance by reducing overshoot and settling time, which enhances stability and more effectively maintains DC link voltage regulation.

The proposed advanced EMS controller overcomes these limitations by integrating a GBO-optimized PI framework with a design objective that explicitly considers harmonic suppression and dynamic response. The GBO-PI tuning ensures that the controller gains are selected to provide aggressive yet stable compensation, enabling rapid error correction in the presence of harmonics, and load-induced disturbances. Furthermore, the optimization accounts for transient performance indices—such as overshoot, settling time, and THD—which collectively allow the EMS controller to achieve enhanced harmonic mitigation, faster transient recovery, and improved overall system stability compared to a standard PI.

### *C. Brief Computational Performance Comparison*

#### *1) Convergence speed*

Convergence, in this context, refers to the point at which an algorithm successfully identifies the optimal fitness value within the specified maximum number of iterations. The convergence plot serves as a key performance indicator for assessing the efficiency and robustness of meta-heuristic optimization algorithms. The proposed algorithm has a significantly lower computational burden than conventional optimization strategies. In terms of iterations required for convergence, GBO-PI converges faster due to its adaptive balance between exploration and exploitation, reaching the optimal solution in only six iterations in Fig 12. By comparison, GJO-PI and HHO-PI show moderate improvement, converging in 14 and 20 iterations, respectively. Meanwhile, PSO-PI exhibits the slowest convergence, requiring 25 iterations to stabilize due to additional parameter tuning—such as velocity and inertia adjustments. This highlights the lower computational burden and superior search efficiency of the GBO framework, which enables rapid identification of optimal PI gains with minimal iterations and reduced computational overhead.

#### *2) Integral Time Absolute Error (ITAE) analysis*

The proposed GBO-PI algorithm achieves the most rapid convergence, s with a minimized fitness value of 0.046705 compared with the other optimizers, presented in Fig. 12. Specifically, it achieves a 90.19% reduction in ITAE relative to the PSO-PI, HHO-PI, and GJO-PI algorithms. The proposed method consistently produced lower ITAE values, indicating faster error decay, smoother transient response, and improved tracking capability. This substantial improvement confirms superior convergence capability, effective tuning, faster error decay, smoother transient response, and improved tracking.

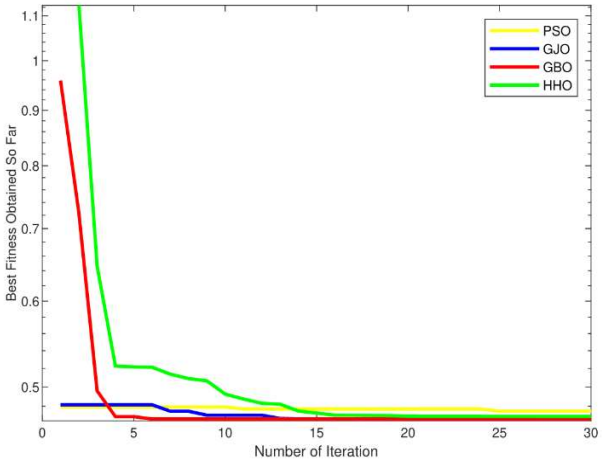


Fig. 12. Proposed GBO and benchmarking PI controllers-based convergence curve for the ITAE Objective function.

#### *3) Stability and robustness*

The proposed GBO-PI controller demonstrates fast, stable convergence and remains robust across varying initial conditions. In contrast, the GA-PI controller converges more slowly due to its selection and crossover processes, offering only moderate stability. The PSO-PI controller requires precise tuning of inertia and velocity coefficients, and its convergence may oscillate if not properly configured. Meanwhile, the GJO-PI controller exhibits slightly slower performance due to its stochastic exploration mechanism, yet maintains overall stability.

#### *4) Execution time*

The proposed GBO-PI shows lower execution time than

GA-PI and GJO-PI, as it avoids complex population update and selection mechanisms inherent in these algorithms. Overall, GBO-PI offers a balanced trade-off between fast convergence, high accuracy, and low computational cost, making it more suitable for real-time DC-link control applications in weak grid conditions. Across all test cases, the proposed method consistently produced lower ITAE values, indicating faster error decay, smoother transient response, and improved tracking capability.

*5) Voltage fluctuation*

The quantitative analysis of ripple voltage clearly demonstrates the superiority of the proposed GBO-PI controller over the existing metaheuristic-based PI controllers. Specifically, it achieves a 60.65% reduction compared to GJO-PI, 55.8% reduction compared to no controller, 55.41% reduction compared to PSO-PI, and 11.79% reduction compared to HHO-PI. These results clearly show that the Proposed GBO-PI provides superior dynamic voltage regulation and more stable DC-link behavior relative to the other optimization-based PI controllers.

*6) Novelty of GBO-PI-optimized strategy in mitigating voltage fluctuations and frequency deviations*

The functional novelty of the proposed GBO-PI strategy lies in its ability to directly enhance EMS stability under weak-grid conditions through an objective function specifically formulated to penalize voltage instability and oscillatory behaviour. By doing so, the GBO optimizer systematically converges toward PI gains that more effectively suppress weak-grid fluctuations. Moreover, the gradient-based component of GBO improves the controller's sensitivity to rapid DC-link disturbances, enabling faster, more accurate error minimization than purely stochastic techniques such as PSO or GA. In addition, the algorithm's mathematical memory mechanism enhances selection pressure and reduces susceptibility to local minima, resulting in more reliable tuning during low-inertia or high-disturbance events. Collectively, these features enable the GBO-PI controller to achieve more stable power-sharing behaviour and superior dynamic tracking performance across a wide range of EMS disturbances. The precise functional novelty of the GBO-PI-optimized strategy lies in its ability to embed weak-grid sensitivity terms directly into its multi-objective cost function and to use a gradient-assisted evolutionary mechanism to minimize DC-link ripple, frequency deviation, and grid-interaction resonance simultaneously. This yields PI gains that actively damp weak-grid oscillations, reduce converter–grid coupling, and minimize harmonic energy transfer—capabilities not achievable through conventional PI tuning or pure metaheuristic approaches.

## V. Conclusion

This paper introduces a control strategy for a single-phase grid-connected fuel cell system, emphasizing the optimization of active and reactive power injection to meet demand requirements through a metaheuristic GBO-PI algorithm. The proposed approach significantly enhances energy management in fuel cell-integrated grid systems by improving DC-link voltage stability, reducing THD, mitigating voltage fluctuations, and ensuring faster convergence. Comparative results demonstrate that GBO-PI delivers superior dynamic performance, enabling rapid system stabilization and outperforming conventional and existing metaheuristic-based controllers. Its effectiveness highlights the potential of metaheuristic optimization in achieving higher power quality and stable grid integration of fuel cell systems. The future study is to develop advanced optimization algorithms, such as hybrid algorithms, to enhance transient response and disturbance rejection capabilities, which are lacking in single-optimization-based algorithms, and to focus on implementing the FC integrated model in hardware.

## Conflict of Interest

The authors declare no conflict of interest.

## Author Contributions

Mohammad G. Mostafa contributed to conceptualization, methodology, and writing – original draft; Nor Zaihar B. Yahaya, Ramani K. and Nursyarizal Bin M. Nor were responsible for supervision, validation, and writing – review & editing; all authors had approved the final version.

## Acknowledgment

This research is conducted under the sponsorship of Universiti Teknologi PETRONAS (UTP), Perak, Malaysia under the Graduate Assistantship (GA) scheme.

## References

[1] P. Phogat, B. Chand, R. Jha, and S. Singh, "Hydrogen and methanol fuel cells: A comprehensive analysis of challenges, advances, and future prospects in clean energy," *International Journal of Hydrogen Energy,* vol. 109, pp. 465–485, 2025. doi: 10.1016/j.ijhydene.2025.02.133

[2] S. M. Hisham, N. Sazali, and M. K. Kamarulzaman, "Exploring hydrogen storage options: A brief review of gaseous, liquid, and solid-state approaches," *Engineering, Technology & Applied Science Research* vol. 14, no. 5, pp. 16580–16585, 2024.

[3] K. B. Samal, S. Pati, and R. Sharma, "Performance analysis of PID and SMC for PEMFC-based grid integrated system using nine switch converter—A comparative study," *Unconventional Resources,* vol. 5, 100108, 2025.

[4] N. Khosravi, D. Çelik, H. Bevrani, and S. Echalih, "Microgrid stability: A comprehensive review of challenges, trends, and emerging solutions," *Electrical Power and Energy Systems,* vol. 170, 11082, Sep. 2025.

[5] E. Hernández-Mayoral, Christian R. Jiménez-Román, Jesús A. Enriquez-Santiago, "Power quality analysis of a microgrid-based on renewable energy sources: A simulation-based approach," *Computation,* vol. 12, no. 11, 226, 2024.

[6] S. T. Meraj, S. S. Yu, and M. M. Hasan, "Advanced energy management scheme for fuel cell-based microgrid using self–regulated controller and switched capacitor inverter," *International Journal of Hydrogen Energy,* vol. 90, pp. 1477–1494, 2024. doi: 10.1016/j.ijhydene.2024.10.085

[7] B. Amini, H. Rastegar, and M. Pichan, "An optimized proportional resonant current controller based genetic algorithm for enhancing shunt active power filter performance," *International Journal of Electrical Power & Energy Systems,* vol. 156, 109738, 2024.

[8] Z. H. Ali and D. Raisz, "Comparative experimental evaluation of three-wire SAPF control strategies for power quality improvement,"

*Energy Reports,* vol. 13, pp. 1332–1349, 2025. doi: 10.1016/j.egyr.2025.01.020
[9] W. Chen, Y. Han, Q. Li, Z. Liu, and F. Peng, "Design of proton exchange membrane fuel cell grid-connected system based on resonant current controller," *International Journal of Hydrogen Energy,* vol. 39, no. 26, pp. 14402–14410, 2014.
[10] N. Kumar and S. K. Panda, "A multipurpose and power quality improved electric vessels charging station for the seaports," *IEEE Trans. on Industrial Informatics,* vol. 19, no. 3, pp. 3254–3261, 2022.
[11] R. Kumar, H. O. Bansal, A. R. Gautam, O. P. Mahela, and B. Khan, "Experimental investigations on particle swarm optimization based control algorithm for shunt active power filter to enhance electric power quality," *IEEE Access,* vol. 10, pp. 54878–54890, 2022.
[12] Q. Li, W. Chen, Z. Liu, G. Zhou, and L. Ma, "Active control strategy based on vector-proportion integration controller for proton exchange membrane fuel cell grid-connected system," *IET Renewable Power Generation,* vol. 9, no. 8, pp. 991–999, 2015.
[13] U. Yilmaz and O. Turksoy, "Artificial intelligence based active and reactive power control method for single-phase grid connected hydrogen fuel cell systems," *International Journal of Hydrogen Energy,* vol. 48, no. 21, pp. 7866–7883, 2023.
[14] B. Liu, G. Li, D. He, and Y. Chen, "DC and AC power quality control for single-phase grid-tied PEMFC systems with low DC-link capacitance by solution-space-reduced MPC," *IEEE Trans. on Industrial Electronics,* vol. 69, no. 6, pp. 5625–5636, 2021.
[15] J. Zhou, Y. Yuan, and H. Dong, "Adaptive DC-link voltage control for shunt active power filters based on model predictive control," *IEEE Access,* vol. 8, pp. 208348–208357, 2020.
[16] M. A. Al-Ani, M. A. Zdiri, F. B. Salem, and N. Derbel, "Optimized grid-connected hybrid renewable energy power generation: A comprehensive analysis of photovoltaic, wind, and fuel cell systems," *Engineering, Technology & Applied Science Research,* vol. 14, no. 3, pp. 13929–13936, 2024.
[17] D. Bakria, A. A. Laouid, and B. Korich, "An optimized shunt active power filter using the golden Jackal optimizer for power quality improvement," *Scientific Reports,* vol. 15, no. 1, 15869, 2025.
[18] M. İnci and Ö. Çelik, "Repetitive control strategy for grid integration of vehicular fuel cells to enhance system stability and robustness," *Journal of Power Sources,* vol. 642, 236992, 2025.
[19] S. Vendoti, N. P. Tulasi, and R. K. Jalli, "Grid tied hybrid PV fuel cell system with energy storage and ANFIS based MPPT for smart EV charging," *Scientific Reports,* vol. 15, no. 1, 27392, 2025.
[20] M. Aminudin, S. Kamarudin, B. Lim, E. Majilan, M. Masdar, and N. Shaari, "An overview: Current progress on hydrogen fuel cell vehicles," *International Journal of Hydrogen Energy,* vol. 48, no. 11, pp. 4371–4388, 2023.
[21] M. Priya and P. Ponnambalam, "Circulating current control of phase-shifted carrier-based modular multilevel converter fed by fuel cell employing fuzzy logic control technique," *Energies,* vol. 15, no. 16, 6008, 2022.
[22] D. Guilbert, B. Nahid-Mobarakeh, S. Pierfederici, N. Bizon, P. Mungporn, and P. Thounthong, "Comparative study of adaptive Hamiltonian control laws for DC microgrid stabilization: An fuel cell boost converter," *Applied Science and Engineering Progress,* vol. 15, no. 3, pp. 5540–5540, 2022.
[23] R. Bisht, S. Subramaniam, R. Bhattarai, and S. Kamalasadan, "Active and reactive power control of single phase inverter with seamless transfer between grid-connected and islanded mode," in *Proc. 2018 IEEE Power and Energy Conference at Illinois (PECI)*, 2018. doi: 10.1109/peci.2018.8334989
[24] T. J. Ypma, "Historical development of the Newton–Raphson method," *SIAM Review,* vol. 37, no. 4, pp. 531–551, 1995.
[25] P. B. Patil and U. Verma, *Numerical Computational Methods*, Alpha Science International, Ltd, 2006.
[26] A. Y. Özban, "Some new variants of Newton's method," *Applied Mathematics Letters,* vol. 17, no. 6, pp. 677–682, 2004.



**Mohammad Golam Mostafa** was born in Dhaka, Bangladesh. He obtained his B.Sc. in electrical and electronic engineering from the University of Asia Pacific (UAP), Dhaka, Bangladesh, in 2010, followed by a master of science in electronics engineering from the International Islamic University Malaysia (IIUM), Kuala Lumpur, Malaysia, in 2015, pursued through by research mode with a thesis titled "Development of Piezoelectric-based DC to DC Converter for Micro Energy Harvesting System". He is currently pursuing a Graduate Assistant (GA) position in Electrical and Electronics Engineering at Universiti Teknologi PETRONAS (UTP), Perak, Malaysia. Since 2018, he has been serving as a Lecturer in the Department of Electrical and Electronic Engineering at the World University of Bangladesh (WUB), Dhaka, Bangladesh, where he is presently on study leave. His research interests include renewable energy, power electronics, energy harvesting, optimization algorithms, converters, inverters, smart grids, and machine learning.

**Nor Zaihar bin Yahaya** was born in Lumut, Perak, Malaysia. He obtained his B.Sc. in electrical engineering from the University of Missouri–Kansas City, USA, in 1996, followed by an M.Sc. in microelectronics from the University of Newcastle upon Tyne, UK, in 2002, and later a Ph.D. in electrical and electronic engineering from Universiti Teknologi PETRONAS (UTP), Malaysia, in 2011. After completing his bachelor's degree, he worked in the industry for about five years before joining academia. He is currently serving as an associate professor at Universiti Teknologi PETRONAS, Perak, Malaysia. Dr. Yahaya has published extensively in journals and conferences, with research contributions spanning power electronics, renewable energy integration, DC–DC converters, multilevel inverters, energy harvesting, and green energy systems. His current research interests include power electronics and drives, renewable energy applications, DC power systems, and energy conversion. He is a Senior Member of IEEE and actively contributes to advancing knowledge in the field through his teaching, research, and publications.

**Ramani Kannan** was born in India. He earned his B.E. in electronics and communication (2004) from Bharathiar University, M.Eng. in power electronics & drives (2006), and Ph.D. in the same field (2012) from Anna University, India. He is currently an associate professor and postgraduate programme leader at Universiti Teknologi PETRONAS (UTP), Malaysia. With over 19 years of academic and research experience, he has led projects in smart battery management, microgrids, and renewable energy, and has published more than 250 papers along with several books. His research interests include power electronics, renewable energy systems, battery management, AI in energy, and radiation effects on devices. He is a Senior Member of IEEE, Chartered Engineer (UK), Professional Technologist (MBOT), and member of IET (UK) and ISTE (India). His recognitions include the AICTE Career Award (2012), Young Scientist Award (2015), UTP Outstanding Researcher Award (2019), and multiple IEEE and UTP awards (2024). He has also held leadership roles in IEEE, guest-edited special issues, and served as reviewer and panel member for journals and grants.

**Nursyarizal bin Mohd Nor** received his diploma (1995) and B.Eng. (1998) in electrical engineering from Universiti Teknologi Malaysia, an M.Sc. in electrical power engineering from UMIST, UK (2001), and a Ph.D. in electrical & electronic engineering from Universiti Teknologi PETRONAS (2009). He is currently an associate professor in the Department of Electrical & Electronics Engineering at UTP, Malaysia. He has published over 100 scholarly works in power system analysis, renewable energy, electrical machines, and power quality. His research interests

include smart grids, state estimation, renewable energy integration, and power system operation. He is a Professional Engineer with Practicing Certificate (PEPC), an ASEAN Chartered Professional Engineer, a corporate member of IEM, and a member of the IEEE Power & Energy Society. He also contributes actively to professional committees, accreditation exercises, and research grant evaluations.